# Reducing Dephosphorization of SiMn Alloy by Molten $CaO-CaF_2$ Flux and Thermodynamic Stability of $Ca_3P_2$ under Atmospheric Cooling Conditions

*Jae Hong SHIN and Joo Hyun PARK**

*School of Materials Science and Engineering, University of Ulsan, Ulsan 680-749, Korea.*

**Abstract:** This study consists of experimental measurement of the phosphide capacity of the $CaO-CaF_2$ flux in equilibrium with SiMn alloy at 1823 K, and includes the thermodynamic analysis of the stability of reducing refining slags under wet atmospheric cooling conditions. The phosphide capacity increased with increasing CaO concentration in the flux, followed by a constant value. The composition for the saturating capacity is in good accordance to the saturation content of CaO in the $CaO-CaF_2$ flux at 1823 K. When the Vee ratio (=$CaO/SiO_2$) of the reducing dephosphorization slag is greater than about 1.35, CaO (lime) and $Ca_2SiO_4$ (dicalcium silicate) phases appeared during cooling cycle based on the $CaO-SiO_2-CaF_2$ phase diagram, resulting in an increase of the evolution rate of $PH_3$ gas due to an increase in the reaction area. However, when the Vee ratio of the slag is lower than about 1.35, $CaF_2$, $Ca_4Si_2F_2O_7$ (cuspidine), and $CaSiO_3$ (wollastonite) phases appeared from the phase diagram, resulting in negligible amount of $PH_3$ evolution during cooling because the reaction between $Ca_3P_2$ and $H_2O$ was restricted to the surface of bulk slag.

**Key words:** Phosphide capacity, $CaO-CaF_2$ slag, Reducing dephosphorization, Phosphine ($PH_3$) gas.

## 1. Introduction

High manganese steels (HMnS, 10~25wt%Mn) are of interest due to their good mechanical properties including superior strength and good ductility.[1-3] Accordingly, the demand for ultra low phosphorous manganese alloys such as FeMn and SiMn alloys has recently increased. However, the conventional oxidizing dephosphorization technique is not applicable to manganese alloys because silicon or manganese will be oxidized before phosphorous is under oxidizing conditions.[4-8] Therefore, the dephosphorization should be carried out under a strongly reducing atmosphere to produce a low phosphorus Mn alloy. The mechanism of reducing dephosphorization has been reported by several authors.[4-11] Although several studies concerning the phosphide capacity of lime-based fluxes have been published, there are few reports of reducing refining of phosphorus from Si-Mn alloys.

In addition, because the $Ca_3P_2$, which is a reaction product of the reducing dephosphorization mechanism, is very active when it contacts to moisture, the phosphine gas ($PH_3$) evolves. The equilibrium reaction of phosphine gas evolution is as follows:

$$Ca_3P_2(s) + 3H_2O(g) = 3(CaO) + 2PH_3(g) \quad [1]$$

$$Ca_3P_2(s) + 6H_2O(g) = 3Ca(OH)_2 + 2PH_3(g) \quad [2]$$

Figure 1 shows the Gibbs free energy change of the formation reaction of phosphine gas, which was calculated using Factsage™6.2, whish is thermodynamic computing program. The evolution of phosphine gas is unavoidable because the Gibbs free energy change of the formation of phosphine gas has very negative values.

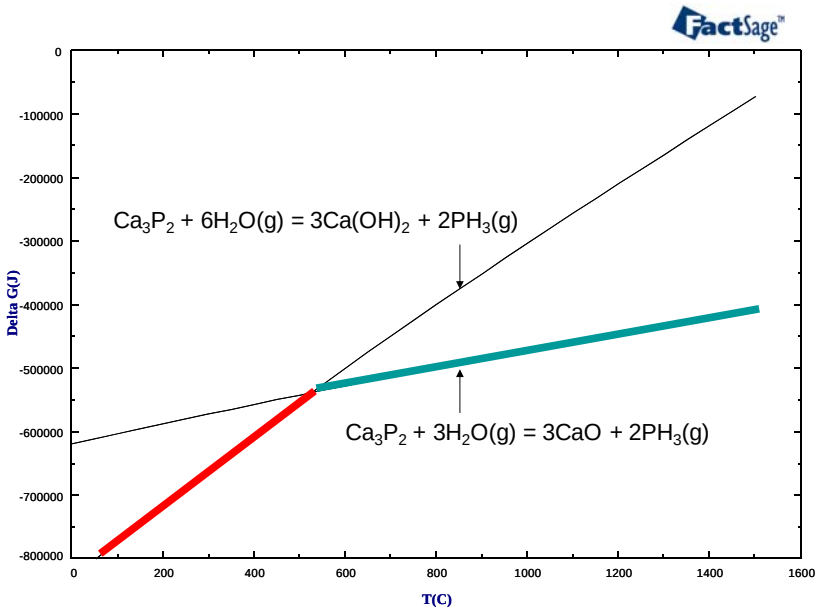


Fig 1. Gibbs free energy change of the formation of $PH_3$ gas by the reaction between $Ca_3P_2$ and $H_2O$ in atmosphere.

Phosphine gas is hazardous to environment as well as to human being. For example, an inhalation is the most likely route of exposure to phosphine.[12] Symptoms are non-specific and include irritation of the respiratory tract, headaches, dizziness, abdominal pain, sickness, and vomiting. Severe phosphine poisoning can cause convulsions, damage to the lungs, heart, liver and kidney, and death.

Therefore, in the present study, we investigated the thermodynamic behavior of phosphide ions in the CaO-$CaF_2$ flux in equilibrium with a Si-Mn alloy melt under a strongly reducing atmosphere, and carried out the thermodynamic analysis for the environmental stability of reducing refining slags under wet conditions based on the effect of slag composition on the evolution of $PH_3$ gas.

## 2. Experimental

A super-kanthal electric furnace was used for the equilibration of the CaO-$CaF_2$ flux and Si-Mn alloy melts. The

temperature was controlled within ±2 K using a B-type thermocouple and a PID controller. The slag samples were prepared using reagent grade $CaF_2$ and CaO calcined from $CaCO_3$ at 1273 K for 10 hours. The experimental composition of the slag in the CaO-$CaF_2$ system ranged from 5 to 25wt% CaO.

The slag (7.0 g) and SiMn alloy (3.5 g) were held in graphite crucibles under a CO atmosphere to equilibrate. For reducing removal of phosphorous under a very low oxygen potential, CO gas was diluted with Ar, which was purified using silica gel also in addition to Mg turnings at 723 K. The oxygen partial pressure can be calculated based on the following reaction.[13]

$$\mathrm{C(s)} + \frac{1}{2}\mathrm{O_2(g)} = \mathrm{CO(g)}, \quad \Delta G^{\mathrm{o}} = -114{,}445 - 85.8T \ \mathrm{(J/mol)} \qquad [3]$$

With a CO/(CO+Ar) ratio of 0.25, the oxygen partial pressure is about $1.7\times10^{-17}$ atm at 1823 K. The CO gas was passed through Drierite®, $Mg(ClO_4)_2$, silica gel, and soda lime to eliminate moisture and impurities. The time to establish equilibrium was preliminarily determined. After equilibrating for 12 hours, the slag samples were cooled under fully moisturized condition (direct contact with water), whereas the other samples were quickly quenched from 1823 K. Then, the samples were rapidly crushed for chemical analysis under inert atmosphere. The composition of metal samples was determined using ICP-AES and the equilibrium composition of slag was determined using XRF. The crystalline phases of solidified slags were identified using XRD analysis.

## 3. Results and discussion

### 3.1. Reducing dephosphorization mechanism of SiMn alloy using CaO-$CaF_2$ flux

Under the highly reducing conditions, phosphorous is expected to dissolve into the flux as phosphide ions as follows:[4-11]

$$[\mathrm{P}] + \frac{3}{2}(\mathrm{O^{2-}}) = (\mathrm{P^{3-}}) + \frac{3}{4}\mathrm{O_2(g)} \qquad [4]$$

$$K_{[4]} = \frac{a_{\mathrm{P^{3-}}} \cdot p_{\mathrm{O_2}}^{0.75}}{a_{\mathrm{P}} \cdot a_{\mathrm{O^{2-}}}^{1.5}} = \frac{\gamma_{\mathrm{P^{3-}}} \cdot X_{\mathrm{P^{3-}}}}{\gamma_{\mathrm{P}} \cdot X_{\mathrm{P}}} \cdot \frac{p_{\mathrm{O_2}}^{0.75}}{a_{\mathrm{O^{2-}}}^{1.5}} \qquad [5]$$

where $a_{\mathrm{P^{3-}}}$ and $\gamma_{\mathrm{P^{3-}}}$ are the activity and the activity coefficient of the phosphide ions in the slag phase, respectively, and $a_{\mathrm{P}}$ and $\gamma_{\mathrm{P}}$ are the activity and the activity coefficient of phosphorous in the SiMn alloy phase, respectively, and

$p_{O_2}$ is the oxygen partial pressure, and $a_{O^{2-}}$ is the activity of free oxygen, i.e. the basicity of slag. In the present study, the dephosphorization efficiency ($\eta_{\text{de-P}}$) is determined from the following equation:

$$\eta_{\text{de-P}}(\%) = \frac{[\text{wt\%P}]^{\text{o}} - [\text{wt\%P}]^{\text{e}}}{[\text{wt\%}]^{\text{o}}} \times 100 \qquad [6]$$

where the superscripts 'o' and 'e' represent the initial and the equilibrium content of phosphorus in the metal, respectively.

Figure 2 shows the effect of the CaO content in the CaO-$CaF_2$ flux on the dephosphorization efficiency of the SiMn alloy at 1823 K. The dephosphorization efficiency increases with increasing CaO content up to about 20wt%, which is due to an increase in the basicity of the flux. However, the dephosphorization efficiency remained constant at CaO content greater than about 20wt%, where the flux is saturated by solid lime from the CaO-$CaF_2$ binary phase diagram,[14] This indicates that the activity of free $O^{2-}$ ions is constant, assuming that $a_{O^{2-}}$ is proportional to $a_{CaO}$ in the flux.[15-20]

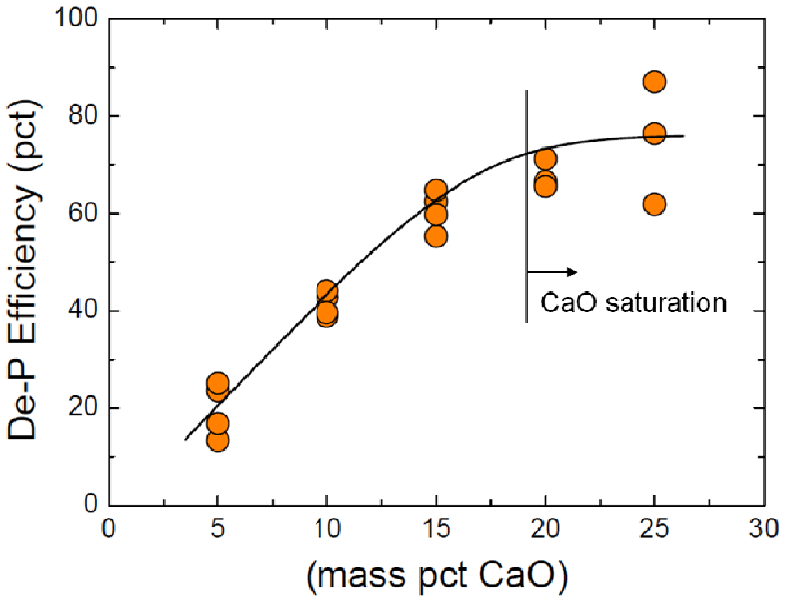


Fig 2. Effect of CaO content on the dephosphorization efficiency of the CaO-$CaF_2$ flux in equilibrium with SiMn melt.

From Eq. [5], the phosphide capacity of the slag can be defined as functions of temperature, basicity, and the stability of phosphide in the slag as follows:

$$C_{P^{3-}} = \frac{K_{[4]} \cdot a_{O^{2-}}^{1.5}}{\gamma_{P^{3-}}} = L_P \cdot \frac{p_{O_2}^{0.75}}{\gamma_P} \quad [7]$$

where $L_P$ is the distribution ratio of P between the slag and metal phases, i.e. $L_P = (X_{P^{3-}}) / [X_P]$. Thus, the phosphide capacity of the slag is expected to increase with increasing basicity. The phosphide capacity of the flux was calculated based on Eq. [7] using the activity coefficient of phosphorus in the metal phase obtained from Eq. [8].[21]

$$\ln \gamma_P = \ln \gamma_{P\ in\ Si}^{o} + \varepsilon_P^{Mn} X_{Mn} + \varepsilon_P^{Fe} X_{Fe} + \varepsilon_P^{Ca} X_{Ca} + \varepsilon_P^{C} X_C \quad [8]$$

where $\gamma_{P\ in\ Si}^{o}$ is the activity coefficient of phosphorous in the silicon melt relative to the infinite dilution condition, $\varepsilon_P^i$ is the interaction parameter between phosphorous and element *i* in the alloy. The $\gamma_{P\ in\ Si}^{o}$ and $\varepsilon_P^i$ values used in the present calculation are listed in Table 1.[22-25]

Table 1. Interaction Parameters and Henrian Activity Coefficient of Phosphorus Used in the Present Study ( $\varepsilon_P^i$ ).

| Element (*i*) | Value | Solvent | Ref. |
|---|---|---|---|
| Mn | 12.0 | Si-Mn ($X_{Mn} \leq 0.5$) | 22 |
| Fe | 7.43 | Si-Fe ($X_{Fe} \leq 0.65$) | |
| Ca | -14.6 | Si-P(-Ca) | 23 |
| P | 13.8 | Si-P(-Ca) | |
| C | 9.86 | Mn-Si(-$C_{sat.}$) | 24 |
| $\ln \gamma^{o}_{P}$ | -0.53 | Si-P | 25 |

The phosphide capacities of various lime-based fluxes and BaO-$BaF_2$ flux are plotted against the molar content of CaO (BaO) in Figure 3. The lime saturation in the CaO-$CaF_2$ flux occurs at 20~25mol% CaO at 1823 K and thus, saturation of the phosphide capacity is expected at this composition because $a_{CaO} = 1$.[14] This means that the reducing refining mechanism was confirmed through the transfer of Ca from the slag to the metal phase due to the reaction between CaO in the flux and Si in the alloy under strongly reducing conditions (Eqs. [9] and [10]).

$$2(CaO) + [Si] = (SiO_2) + 2[Ca] \quad [9]$$

$$3[Ca] + 2[P] = (Ca_3P_2) \quad [10]$$

This tendency is in good agreement with the results reported by Tabuchi and Sano.[5] However, despite the fact that the same flux was used, our results are lower than Tabuchi and Sano's work. They calculated the phosphide capacity using the standard free energy of dissolution of phosphorous in a silver melt. However, in the present study, the phosphide capacity of the flux was calculated using the activity coefficient of phosphorous in the SiMn(-Fe-C) melt based on the interaction parameters between phosphorous and each element. Consequently, the discrepancies between both studies may be due to thermodynamic uncertainties in the activity coefficients of phosphorous in the Ag and Si-Mn(-Fe-C) melts.[7,26]

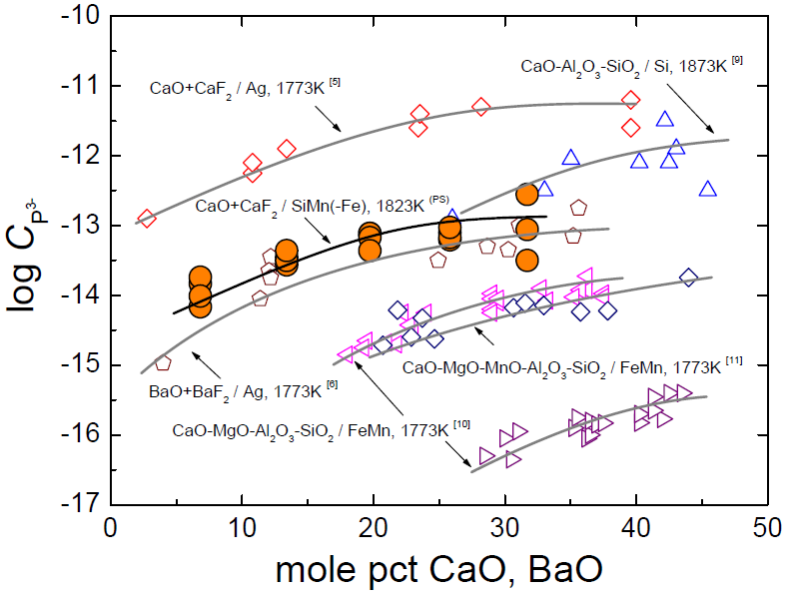


Fig 3. Phosphide capacity of various flux systems as a function of molar content of basic oxide (PS; present study).

Fujiwara *et al.*[9] measured the phosphide capacity of the CaO-$Al_2O_3$-$SiO_2$ slag system in equilibrium with the Si base alloy melt at 1873 K. The phosphide capacity of the CaO-$Al_2O_3$-$SiO_2$ slag is higher than that of the CaO-$CaF_2$ slag, which is due to the higher CaO content in the former system. The phosphide capacity of the CaO-$SiO_2$-MgO-$Al_2O_3$(-MnO) slags at 1773 K measured by Eric *et al.*[10,11] at $p(O_2)=1.2\times10^{-16}$ atm is similar to that obtained in this study. They also measured the phosphide capacity of the CaO-$SiO_2$-MgO-$Al_2O_3$ slag at 1773 K and $p(O_2)=7.8\times10^{-19}$ atm, which resulted in a lower capacity for the same slag system. This discrepancy for the same flux system originates from the difference in the oxygen potentials.[10,11]

Because of the experimental difficulty in producing phosphorous vapor, which was originally experienced by

Tabuchi and Sano,[5,6] the phosphide capacity of the slags is generally calculated from the distribution ratio of phosphorous between the metal and slag, the activity coefficient of phosphorous in the metal phase, and the oxygen potential (Eq. [4]). Consequently, despite the fact that the capacity is an inherent and unique property of molten slag at a given temperature, the phosphide capacity is inevitably influenced not only by the activity coefficient of phosphorous in the metal phase but also by the oxygen potential.[7,26]

### 3.2. Influence of CaO content on the evolution of $PH_3$ gas

If all of phosphide that transferred from metal to slag were reacted with moisture, the amount of phosphine gas formed was calculated by difference in the phosphorous content in slag before and after reaction. According to Eq [1], the driving force of forward reaction increases with increasing partial pressure of $H_2O$, whereas it decreases with increasing activity of CaO. Thus, the evolution of phosphine gas is affected by above two factors.

Figure 4 shows the effect of CaO content on the amount of phosphine gas evolved which was normalized with reference to the quenched sample. In the lower CaO content region, viz. $a_{CaO} < 1$, the phosphine gas was evolved due to the large potential of $H_2O$ which is greater than that of CaO. However, in the higher CaO content region, viz. $a_{CaO} = 1$, the phosphine gas is still evolved, which is different from the thermodynamic expectation. The reason for this finding is discussed in the following sections.

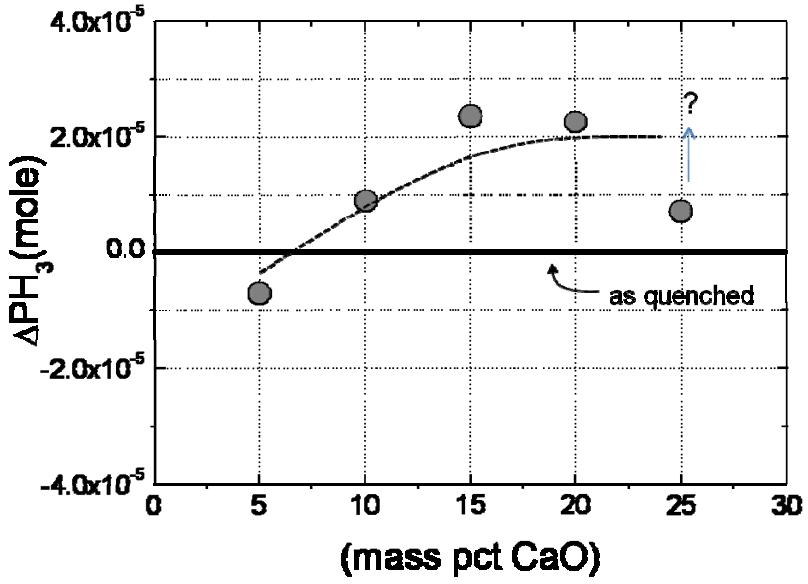


Fig 4. The effect of CaO content in the slag on the evolution of phosphine gas during cooling under wet conditions.

### 3.3. Influence of disintegration of slag on the evolution of $PH_3$ gas

Figure 5 shows the morphology of slag samples after experiment. When the CaO content is greater than about 20wt%, the slag was disintegrated into fine powders during cooling. The powdery slag in the $CaO\text{-}CaF_2\text{-}SiO_2$ slag is formed by two factors. Firstly, if CaO (lime) is precipitated during solidification under wet conditions, the hydration of CaO occurs, resulting in the volume expansion of slag.[27,28] Secondly, if $Ca_2SiO_4$ (dicalcium silicate) is precipitated during solidification, the $Ca_2SiO_4$ contributes to powdery slag because of the volume expansion by the phase transformation of $Ca_2SiO_4$ from β- to γ-phase at about 773 K.[29]

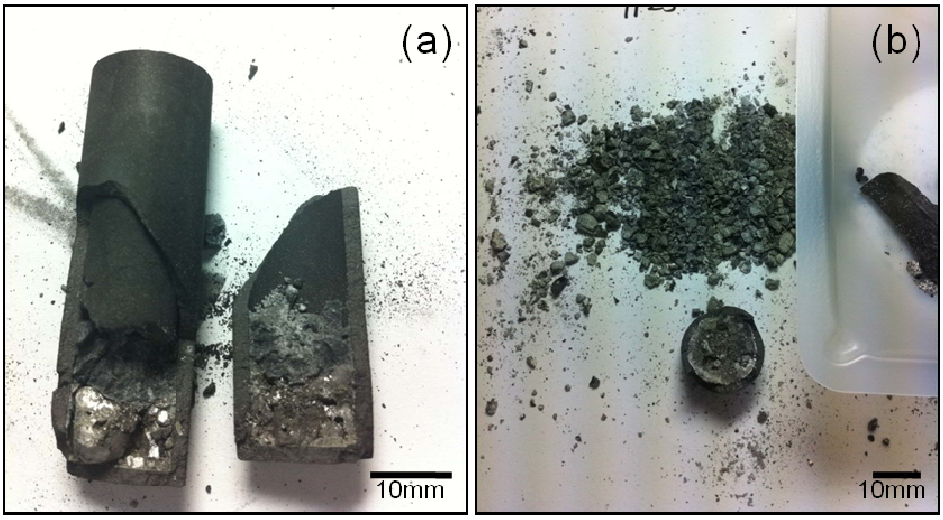


Fig 5. Morphology of the low (5wt%) (a) and high (25wt%) CaO samples after experiment.

Generally, the rate equation is functions of reaction surface area and driving force such as difference in concentration. Thus, the larger the surface area, the faster the reaction will occur. That is, a disintegration of slag to fine powders results in a significant increase in surface area. The rate equation of the evolution of phosphine gas is as follows:

$$-\frac{d(C_{PH_3})}{dt} = \frac{A}{V} \cdot k_m \cdot (C^{o}_{PH_3} - C^{e}_{PH_3}) \qquad [11]$$

where $k_m$ is rate constant, $A$ and $V$ are surface area and volume, respectively. $C_{PH_3}$ is concentration of phosphine gas and the superscripts ‘o’ and ‘e’ represent the initial and the equilibrium concentration, respectively. The surface area of powdery slag, which is constituted by large and small spherical particles, can be calculated by Eq [12].[30]

$$A = \frac{X_S \cdot (V \times f)}{V_S} \cdot A_S + \frac{X_L \cdot (V \times f)}{V_L} \cdot A_L \qquad [12]$$

where $X_{L\,or\,S}$ is mole fraction of large or small particles, $V$ is volume of bulk state, and $V_{L\,or\,S}$ and $A_{L\,or\,S}$ are volume and area of unit of large or small particles, respectively. $f$ is powder packing factor. For two spherical powder with a large difference in particle size with an ideal fractional density of 0.637,[30] the powder packing factor $f$ that function of $X_S$ is determined as follows:

$$f = 0.637 + 0.864\, X_S \qquad [13]$$

Hence, the reaction rate of phosphine gas evolution of powdery slag is determined by combining Eqs. [11] to [13].

$$\frac{1}{Q} \cdot \frac{d(C_{PH_3})}{dt} = \frac{(r_S + (r_L - r_S) \cdot X_S) \cdot (0.637 + 0.864 X_S)}{r_L \cdot r_S} \qquad [14]$$

where $Q$ is constant, and $r_{L\,or\,s}$ is radius of large or small particles.

Figure 6 shows the effect of particle size and the mole fraction of small particle on the evolution rate of phosphine gas. The more the slags become powdery, the larger the reaction surface area is expected, and thus the rate of gas evolution increases as a quadratic function. Therefore, if CaO or $Ca_2SiO_4$ is crystallized during solidification, the phenomena of slag disintegration are occurred.

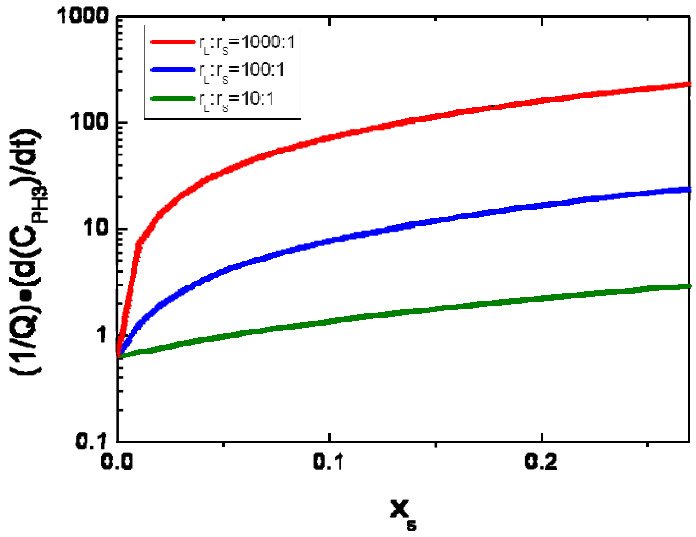


Fig 6. The effect of particle size and mole fraction of small particles on the evolution rate of phosphine gas.

### 3.4. Solidification path of slag and the evolution of $PH_3$ gas

Table 2 shows the slag composition before and after dephosphorization reaction. The content of $SiO_2$ increased due to slag-metal reaction which is given in Eq. [9]. The slag composition after dephosphorization is plotted on the $CaO$-$CaF_2$-$SiO_2$ ternary phase diagram as shown in Figure 7.[31]

Table 2. Slag composition before and after dephosphorization reaction in the present study.

| Sample | Before De-P | | After De-P | | | | |
|---|---|---|---|---|---|---|---|
| No. | $CaF_2$ | CaO | $CaF_2$ | $SiO_2$ | `CaO | MnO | $Fe_2O_3$ |
| **Q1** | 95 | 5 | 96.5 | 3.6 | - | 0.3 | 0.2 |
| **Q2** | 90 | 10 | 93.7 | 3.9 | 1.2 | 0.3 | 0.2 |
| **Q3** | 85 | 15 | 86.0 | 5.2 | 7.7 | 0.5 | 0.2 |
| **Q3** | 80 | 20 | 75.8 | 8.4 | 14.1 | 0.8 | 0.2 |

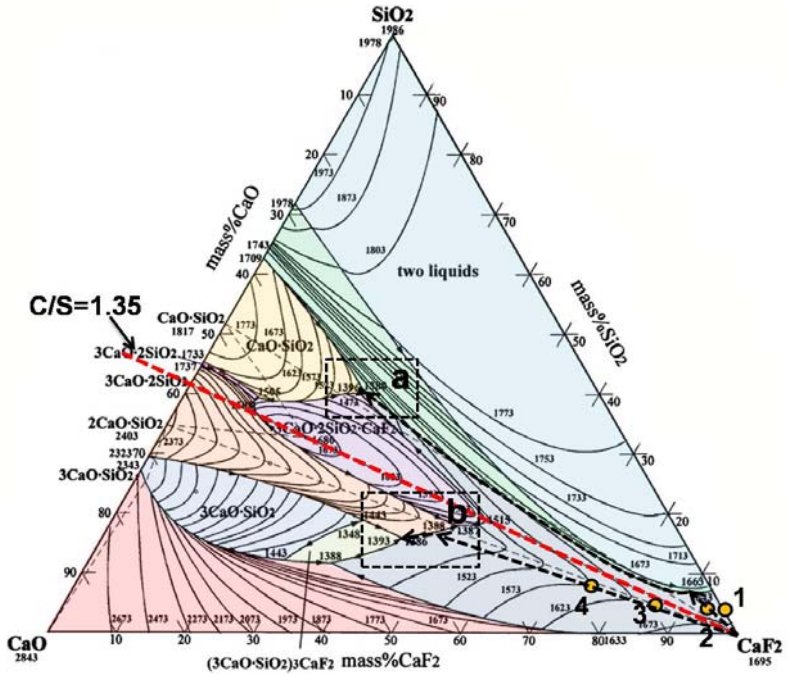


Fig 7. Slag composition after dephosphorization, #1 to #4 in the $CaO$-$CaF_2$-$SiO_2$ ternary phase diagram.[31]

Solidification path can be predicted based on the $CaO$-$CaF_2$-$SiO_2$ ternary phase diagram and Figure 8 shows schematic diagram of cooling path and the microstructure of solidified slag in each case ‘a’ and ‘b’ in Figure 7. For slags of #1 and #2, the $CaF_2$ is primarily crystallized, followed by the nucleation and growth of silica. After that, the pseudo-wollastonite nucleated and finally the slag solidifies at the $CaF_2$-$CaSiO_3$-$3CaO.2SiO_2.CaF_2$ ternary eutectic composition. That is, in view of kinetics, the rate of phosphine gas evolution is relatively low, because the solid compound that contributes to the disintegration are not precipitated.

On the other hand, for slags of #3 and #4, the $CaF_2$ is primarily crystallized, followed by the nucleation and growth

of $Ca_2SiO_4$. After that, slag solidifies at the $CaF_2$-$Ca_2SiO_4$-$(3CaO.SiO_2)_3CaF_2$ ternary eutectic composition. That is, the rate of phosphine gas evolution is relatively high, because the solid compound that contributes to the disintegration of slag, e.g. $Ca_2SiO_4$ is precipitated.

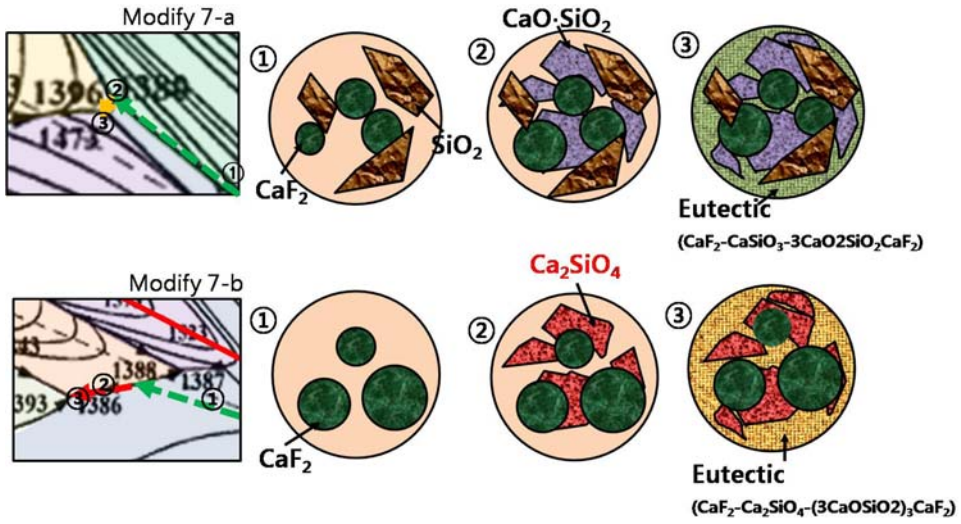


Fig 8. Schematic diagram of the cooling path and the microstructure of solidified slags.

Consequently, when the Vee ratio of the dephosphorization slag is greater than about 1.35, the lime and dicalcium silicate phases appeared during cooling cycle. However, when the Vee ratio of the slag is lower than about 1.35, the $CaF_2$, $Ca_4Si_2F_2O_7$ (cuspidine), and $CaSiO_3$ (wollastonite) and $SiO_2$ phases appeared.

Figure 9 shows the result of XRD analysis of dephosphorization slag that initial composition is 5wt% and 25wt% CaO, respectively. The solid compounds at low CaO content slag were identified as mostly $CaF_2$, whereas teh compounds at high CaO content slag were confirmed to not only $CaF_2$ but also CaO and $Ca_2SiO_4$. Thus, the thermodynamic considerations are in good agreement with the experimental data in this study.

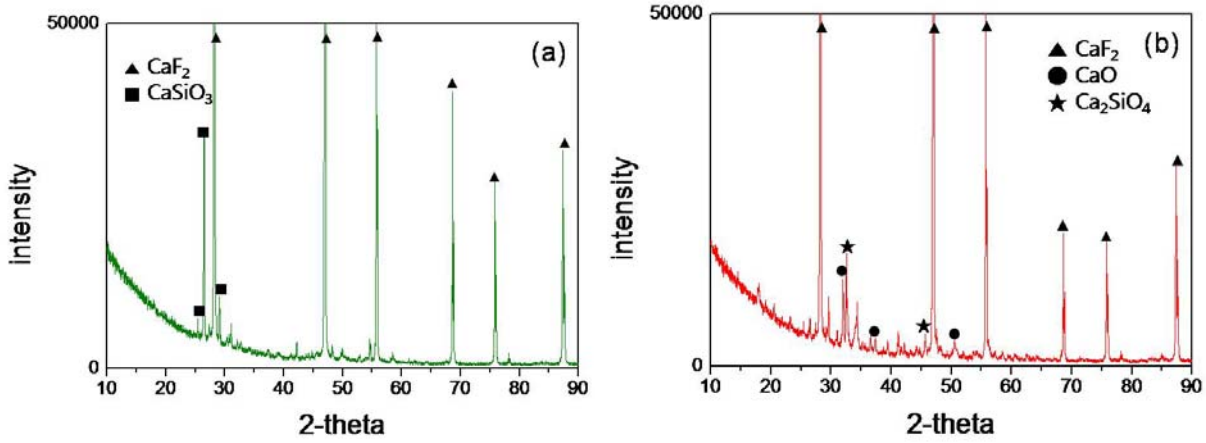


Fig 9. XRD analysis of dephosphorization slag. (a) initial CaO content 5wt%, (b) initial CaO content 25wt%.

Therefore, when the Vee ratio (=$CaO/SiO_2$) of the dephosphorization slag is greater than about 1.35, the evolution rate of $PH_3$ gas increases due to an increase in the reaction area. However, when the Vee ratio of the slag is lower than about 1.35, the amount of $PH_3$ evolution during cooling is negligible because the reaction between $Ca_3P_2$ and $H_2O$ was restricted only to the surface of bulk slag.

## 4. Conclusions

The dephosphorization efficiency increased with increasing CaO concentration in the flux, followed by a constant value. The composition for the saturating dephosphorization efficiency is in good accordance to the saturation content of CaO in the CaO-$CaF_2$ flux at 1823 K. This means that the reducing refining mechanism was confirmed due to transfer of Ca from slag to metal phase by the reaction between CaO in the flux and Si in the alloy under strongly reducing conditions. When the dephosphorization slag was disintegrated into fine powders not only due to the phase transformation of dicalcium silicate but also due to the hydration of lime in the highly basic flux, the evolution of phosphine gas significantly increased. When the Vee ratio (=$CaO/SiO_2$) of the dephosphorization slag is greater than about 1.35, the CaO (lime) and $Ca_2SiO_4$ (dicalcium silicate) phases appeared during cooling cycle based on the CaO-$CaF_2$-$SiO_2$ phase diagram, resulting in an increase in the evolution rate of $PH_3$ gas due to an increase in the reaction area. However, when the Vee ratio of the slag is lower than about 1.35, the $CaF_2$, $Ca_4Si_2F_2O_7$ (cuspidine), and $CaSiO_3$ (wollastonite) phases appeared from the phase diagram, resulting in negligible amount of $PH_3$ evolution during cooling because the reaction between $Ca_3P_2$ and $H_2O$ was restricted to the surface of bulk slag. Therefore, the Vee ratio of dephosphorization slag should be controlled to be lower than 1.35 for retraining phosphine gas evolution.

## References


[1] K.H. So, J.S. Kim, Y.S. Chun, K.T. Park, Y.K. Lee and C.S. Lee. Hydrogen delayed fracture properties and internal hydrogen behavior of a Fe-18Mn-1.5Al-0.6C TWIP steel. *ISIJ Int.*, 2009, 49 (12), p.1952-1959.

[2] Y. Sutou, N. Kamiya, R. Umino, I. Ohnuma and K. Ishida. High-strength Fe-20Mn-Al-C-based alloys with low density. *ISIJ Int.*, 2010, 50 (6), p.893-899.

[3] Y. Lu, D.A. Molodov, and G. Gottstein. Correlation between Microstructure and Texture Development in a Cold-rolled TWIP Steel. *ISIJ Int*., 2011, 51, p.812-817.

[4] H. Momokawa and N. Sano. The effect of oxygen potential on phosphorus in the calcia-alumina system. *Metall. Trans. B*, 1982, 13B, p.643-644.

[5] S. Tabuchi and N. Sano. Thermodynamics of phosphate and phosphide in CaO-$CaF_2$ melts. *Metall. Trans. B*, 1984, 15B, p.351-356.

[6] S. Tabuchi and N. Sano. Thermodynamics of phosphate and phosphide in BaO-$BaF_2$ melts. *Tetsu-to-Hagane*, 1985, 71 (6), p.687-692.

[7] E. Aida, D.J. Min and N. Sano. Phosphorous Distribution between Mn-Si Melts and CaO-$SiO_2$-$CaF_2$ Slags. *Tetsu-to-Hagane*, 1988, 74 (6), p.1931-1938.

[8] N. Sano, W.K. Lu, P.V. Riboud and M. Maeda. *Advanced Physical Chemistry for Process Metallurgy (Chapter 2)*, Academic Press, San Diego, CA, 1997.

[9] H. Fujiwara, J.Y. Liang, K. Takeuchi and E. Ichise. Reducing Removal of Phosphorous from Calcium Containing Silicon Alloys. *Mater. Trans. JIM*, 1996, 37 (4), p.923-926.

[10] B. Maramba and R.H. Eric. Phosphide capacities of ferromanganese smelting slags. *Min. Eng*, 2008, 21, p.132-137.

[11] H. Saridikmen, C.S. Kucukkaragoz and R.H. Eric. Phosphide and Sulphide Capacities of Ferromanganese Smelting slags. *Proc. 8th Int. Conf. on Molten Slag, Fluxes and Salts (MOLTEN2009),* 2009, Santiago, Chile.

[12] L Assem, M Takamiya. HPA Compendium of Chemical Hazards Phosphine. *Institute of Environment and Health* 2007, version 1.

[13] E.T. Turkdogan. *Physical Chemistry of High Temperature Technology*, Academic Press, New York, NY, 1980, p.1-24.

[14] W.G. Seo, D. Zhou and F. Tsukihashi. Calculation of Thermodynamic Properties and Phase Diagrams for the $CaO-CaF_2$, BaO-CaO and $BaO-CaF_2$ Systems by Molecular Dynamics Simulation. *Mater. Trans*., 2005, 46 (3), p.643-650.

[15] S.H. Lee, S.M. Moon, J.H. Park and D.J. Min. Thermodynamic behavior of nickel in $CaO-SiO_2-Fe_tO$ slag. *Metall. Mater. Trans. B*, 2002, 33B, p.55-59.

[16] J.H. Park and D.J. Min. Carbide Capacity of $CaO-SiO_2-CaF_2(-Na_2O)$ Slags. *ISIJ Int.*, 2004, 44, p.223-228.

[17] J.H. Park and D.J. Min. Effect of $ZrO_2$ Addition to the $CaO-SiO_2-MgO-CaF_2$ Slags on the Sulfur Removal from the 16Cr-14Ni Stainless Steel Melts. *Mater. Trans.*, 2006, 47, p.2038-2043.

[18] J.H. Park, G.H. Park and Y.E. Lee. Carbide Capacity of $CaO-SiO_2$-MnO Slag for the Production of Manganese Alloys. *ISIJ Int*., 2010, 50, p.1078-1083.

[19] G.H. Park, Y.B. Kang and J.H. Park. Sulfide Capacity of the $CaO-SiO_2$-MnO Slag at 1873K. *ISIJ Int*., 2011, 51, p.1375-1382.

[20] K.Y. Ko and J.H. Park. Dissolution Behavior of Indium in the $CaO-SiO_2-Al_2O_3$ *Metall. Mater. Trans. B*, 2011, 42B, p. 1224-1230.

[21] C.H.P. Lupis. *Chemical Thermodynamics of Materials*, Prentice Hall, New York, NY, 1993, p.252-255.

[22] S. Ueda, K. Morita and N. Sano. Thermodynamics of Phosphorus in Molten Si-Fe and Si-Mn Alloys. *Metall. Mater. Trans B*, 1997, 28B, p.1151-1154.

[23] T. Shimpo, T. Yoshikawa and K. Morita. Thermodynamic Study of the Effect of Calcium on Removal of Phosphorus from Silicon by Acid Leaching Treatment. *Metall. Mater. Trans B*, 2004, 35B, p.277-284.

[24] S.C. Shim, K. Morita and N. Sano. Thermodynamics of phosphorus in carbon-saturated manganese based alloys. *J. Kor. Inst. Metall. Mater*, 1999, 37 (2), p.244-250.

[25] A.I. Zaitsev, N.E. Shelkova and A.A. Kodentsov. Thermodynamic properties and phase equilibria in the silicon-phosphorus system. *J. Phase Equilib.,* 2000, 21 (6), p.528-533.

[26] K. Morita. Private communication, November 2011.

[27] D. Min, H. Dongwen, L. Xianghui, T. Mingshu. Mechanism of Expansion in Hardened Cement Pastes With Hard-Burnt free lime. *Cement Concrete Res.,* 1995, 25 (2), p.440-448.

[28] E. Serris, L. Favergeon, M. Pijolat, M. Soustelle, P. Notier, R.S. Garter, T. Chopin, Z. Habib. Study of the hydration of CaO powder by gas-solid reaction. *Cement Concrete Res.,* 2011, 41, p.1078-1084

[29] C. Remy, D. Andrault. High-Temperature, High-Pressure X-ray Investigation of Dicalcium Silicate. *J. Am. Ceram. Soc*, 1997, 80 (4), p.851-860.

[30] R.M. German.*Powder Metallurgy Science,* Metal Powder Industries Federation, New Jersey, 1994, p. 166-171.

[31] T. Watanabe, H. Fukuyama, K. Nagata. Stability of Cuspidine ($3CaO{\cdot}2SiO_2{\cdot}CaF_2$) and Phase Relations in the $CaO-SiO_2-CaF_2$ System. *ISIJ Int.*, 2002, 42 (5), p.489-497.